Glassy relaxation and excess wing in mode-coupling theory: The dynamic susceptibility of propylene carbonate above and below T_c

Markus Domschke,[1] Mie Marsilius,[1] Thomas Blochowicz,[1] and Thomas Voigtmann[2,3]
[1]*Institut für Festkörperphysik, Technische Universität Darmstadt, D-64289 Darmstadt, Germany*
[2]*Institut für Materialphysik im Weltraum, Deutsches Zentrum für Luft- und Raumfahrt (DLR), D-51170 Köln, Germany*
[3]*Zukunftskolleg und Fachbereich Physik, Universität Konstanz, D-78457 Konstanz, Germany*
(Received 8 July 2011; published 30 September 2011)

We explore the possibility of describing experimental susceptibility spectra of the glass former propylene carbonate with a two-component schematic model of mode-coupling theory (MCT) from above the melting point down to temperatures far below the critical temperature of MCT. By introducing a phenomenological time-dependent hopping rate, the spectra are reproduced in the full frequency and temperature range available. Literature data of dielectric susceptibilities and depolarized Brillouin light-scattering spectra are combined with our measurements of photon correlation spectroscopy to cover up to 18 decades in frequency of spectra for two different dynamical variables. A consistent description of all data sets is obtained by adjusting only a few physically motivated parameters. In particular the excess wing or slow β-relaxation commonly observed in the susceptibility spectra can consistently be modeled as originating from a coupling of the individual experimental probe correlator to the collective density fluctuations.

DOI: 10.1103/PhysRevE.84.031506 PACS number(s): 64.70.pm, 61.20.Lc

I. INTRODUCTION

The dynamic susceptibility spectra of glass-forming systems present a major challenge for any theory aiming at a quantitative description of the slow dynamics in supercooled liquids [1,2]. Probed by a combination of relaxation and scattering techniques, they show nontrivial features spanning the whole accessible frequency range, from a few μHz to the THz regime of "microscopic" inter- and intramolecular excitations [3]. A prominent feature is the final, low-frequency relaxation peak termed α-relaxation that shows significant stretching, i.e., is much broader than a simple Debye relaxation. It is characterized by a relaxation time τ_α that dramatically shifts to longer times when lowering the temperature T or, more generally, upon changing control parameters that finally lead to the formation of a glass. At the conventional glass-transition temperature T_g, the α-relaxation by definition is 14 orders of magnitude slower than the microscopic motion. At that point, however, it should be kept in mind, that in general "the" α-peak does not exist; position, strength, and shape rather depend on the measurement technique. It therefore does not make sense to try to assign universal parameters to these features of the α-relaxation, and a theory needs to account for both the universal aspects of glassy dynamics and the nonuniversal features induced by different probes.

Relaxation and scattering experiments that probe the relevant frequency range often uncover a secondary relaxation peak, termed "slow β"-relaxation, that peels off the high-frequency side of the α-peak and exhibits a much weaker temperature dependence. Traditionally, one has distinguished glass formers that instead of the slow β-peak show an anomalous "wing" at the high-frequency side of the α-peak, but there now appears to be a consensus that both cases should be attributed to the same phenomenon [4,5].

At high T, the α-peak separates from the microscopic band, revealing an intermediate minimum in the GHz and MHz range that is much enhanced if one compares with the naïve expectation of a superposition of the microscopic Raman band and the α-/slow β-peaks. In fact, the low- and high-frequency sides of this minimum can be described by power laws ω^{-b} and ω^{a}, respectively. The regime around the minimum is somewhat confusingly also referred to as the β-relaxation regime, sometimes called the "fast β"-regime if the need of distinction arises.

The identification of this β-minimum regime and the explanation of its characteristic power laws has been the first major success of the mode-coupling theory of the glass transition (MCT). The fractal relaxation is understood from the theory as arising from the "cage effect", where molecular motion collectively slows down mainly through nearest-neighbor steric hindrance. The minimum frequency position $\omega_{\min}$ is identified with a typical cage relaxation, and the α-peak as the relaxation mode by which particles escape their cages. In particular, MCT puts a theoretical basis to the ω^{-b} power law describing the initial cage-escape dynamics, known long before only empirically as von Schweidler's law [6]. The asymptotic scaling forms of MCT are convincingly demonstrated by various relaxation and scattering data around the β-minimum at not too low temperatures [1,2].

MCT provides microscopically justified equations of motion that arise from the assumption that the main relaxation modes are those fluctuating forces driven by pairs of density fluctuations. The theory then predicts that caging can become so strong that below a critical temperature T_c, these dynamical modes no longer allow a relaxation to an ergodic liquid state. This implies $\tau_\alpha \to \infty$ and a spectrum that in the limit of low frequencies is characterized by white noise, $\chi''(\omega) \propto \omega$. The idealized glass transition temperature T_c can be identified from experimental data through the scaling relations that MCT predicts for the β-minimum position and height, or for the position of the α-peak above T_c.

Fierce debates have been provoked by the fact that this description of glassy dynamics is no longer fully adequate for

$T < T_c$, and that T_c is typically found significantly above the phenomenological and technically relevant glass transition T_g. While for $T > T_c$, MCT has repeatedly and successfully been used to quantitatively describe the available data [1,2], below T_c the theory captures only some aspects of the dynamics, such as a nontrivial rise in the α-relaxation strength [7–16] or the boson peak occurring at high frequencies [17]. The predicted divergence of τ_α as $T \to T_c$ is not observed experimentally. Consequently, standard MCT cannot be used to describe the complex α-relaxation shapes below T_c.

The common interpretation of T_c is that it marks the change from liquid-like transport above T_c to hopping-mediated solid-like transport below. This is, for example, backed by recent studies of tracer diffusion in metallic melts spanning a huge temperature and diffusivity range [18]: Below T_c, diffusion coefficients of various tracer atoms differ greatly and essentially follow Arrhenius laws with rather different activation energies. Above T_c, the values merge and follow, within experimental accuracy, the same temperature dependence, indicative of MCT's collective caging motion.

Thus, generally, "hopping" motion is thought to be responsible for the dynamics below T_c, and concluded to be lacking in the framework of MCT due to its pair-density approximation. However, to paraphrase Kivelson and Tarjus [19], it is not clear as to what hops over what. Extensions of MCT to include additional "hopping" relaxation processes have been discussed soon after the theory emerged [20], but for various reasons these have not been generally applied. Extended MCT scaling laws have been used [21,22], as well as schematic models [23–26] that include an *ad hoc* hopping parameter [27]. The equations used there have recently also been rederived in an attempt to reconcile MCT with the random first-order theory of the glass transition [28]. Since no viable microscopic approximation for the additional hopping term in the MCT equations was available, these studies approximated it by a Markovian rate, and were consequently limited to discussing deviations from the idealized MCT scaling around the β-minimum due to hopping. They could show that even hopping rates that increase Arrhenius-like at large temperatures, and thus at first glance seem to become so strong as to dominate even in the high-temperature regime, leave the MCT scenario intact for $T > T_c$ [27]. However, this approach could not address the nontrivial α- and slow β-relaxations below T_c, since the Markovian hopping rate ultimately implies Debye-type relaxation.

Some extensions of MCT merit further discussion. Extending the schematic model [27], Chong [29] has derived a semiempirical but microscopic MCT with hopping term, and was able to make parameter-free predictions that have been able to explain the decoupling of diffusion processes from the collective motion (called the Stokes-Einstein violation). Recently, features of a so-called fragile-to-strong crossover found in a number of experiments have been analyzed within this theory [30,31].

The generic form of the equations of motion used in some extended-MCT models has been questioned [32] on the basis of generalized fluctuating hydrodynamics. This critique does not appear to apply strictly to the form used in the above-mentioned models [20,27,29]. Based on this critical assessment of the equations of motion, an alternative hopping model has been proposed by Greenall and Cates [33]. It is based on a decay of the vertex with time, reducing the original quadratic coupling that is responsible for the MCT glass transition sufficiently strongly to avoid the singularity at T_c. Another approach to incorporate ergodicity-restoring effects is based on a continued-fraction representation of the correlation function [34].

In the present paper we follow more closely the original MCT proposal [20], but amend it introducing a time-dependent hopping rate. The proposed model, although probably too simplistic to accurately describe real-world data, is shown to have some of the generic features of glassy relaxation below T_c, in particular non-Debye α-relaxation and the possible emergence of a slow β-process. Thus, in a second step, we develop a more empirical version of the model's equations to test our ideas and demonstrate that one is then able to quantitatively describe essentially all relaxation spectra of a prototypical glass former, propylene carbonate. To this end, we have performed new light-scattering experiments using photon correlation spectroscopy (PCS) probing long times and low frequencies. Our data are then combined with available Brillouin light-scattering data at high frequencies, and compared with broadband dielectric spectroscopy data, in order to provide a generic picture of the dynamics in a typical glass former spanning all the relevant variation in frequency and temperature, from the microscopic band to the α-peak, and from T far above the melting temperature down to T_g.

This paper is organized as follows: In Sec. II we describe the experimental setup and data analysis methods. Section III introduces the extended MCT model and discusses some generic features that emerge from it. Section IV is devoted to an analysis of experimental data within the proposed model, and Sec. V concludes.

II. EXPERIMENTAL RESULTS

Propylene carbonate ($T_g = 157$ K [35], $T_m = 218$ K) with a purity of 99.5% was purchased from Sigma-Aldrich. Since even small amounts of water or other impurities are precipitated on cooling down and turn the sample turbid, the substance was dried at least for 24 hours on a molecular sieve to eliminate water. Following this procedure the sample was filtered under an atmosphere of dried nitrogen gas several times, using hydrophilic 200 nm and 20 nm teflon (PTFE) filters. Moreover the sample was degassed over several pump-and-freeze cycles before it was sealed in a cylindrical cuvette.

Depolarized photon correlation spectroscopy (PCS) experiments were performed in VH mode using a HeNe laser, a Glan-Taylor polarizer, and Glan-Thompson analyzer (extinction $<10^{-6}$). The sample was mounted in a Cryovac cold-finger nitrogen cryostat that gives access to a temperature range from 77 K to 475 K. The scattered light is collected by a "three-mode" optical fiber that is coupled to a Perkin Elmer avalanche photo diode. To obtain the autocorrelation function of the scattered light intensity, an ALV5000 correlator card with a minimum lag time of 200 ns was used.

In PCS the autocorrelation function of the scattered light intensity $g_2(t)$ is related to the correlation function of the

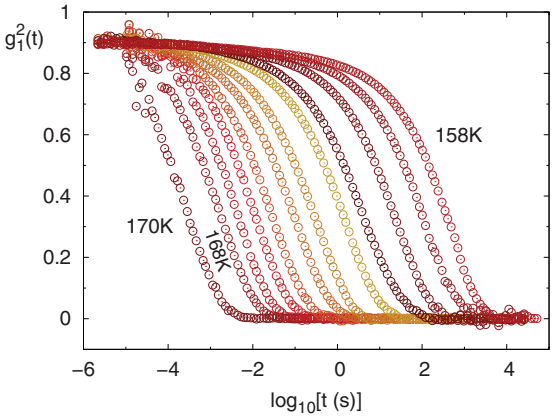

FIG. 1. (Color online) Depolarized correlation functions $g_1^2(t)$ obtained by photon correlation spectroscopy on propylene carbonate. Temperature decreases from 170 K to 158 K from left to right, below 168 K in steps of 1 K.

electric field $g_1(t)$ via the Gaussian approximation $g_2(t) = 1 + \Lambda g_1^2(t)$. In our case a spatial coherence factor of $\Lambda = 1/3$ has to be considered, due to the mentioned three-mode fiber optics system. Figure 1 shows intensity correlation functions of depolarized scattering $g_2(t) - 1$ corrected for the spatial coherence factor from $T = 170$ K down to $T = 158$ K $\approx T_g$. Since in depolarized mode propylene carbonate scatters with very low intensity, it was not possible to use the quasi-cross-correlation technique in order to suppress after-pulsing effects. Instead, the data were corrected for after-pulsing according to a method suggested by Zhao *et al.* [36].

In order to combine our time-domain PCS data with frequency-domain light-scattering measurements in the GHz–THz range from the literature [37], the PCS data were numerically Fourier-transformed,

$$\chi_{\mathrm{LS}}(\omega) = \frac{1}{2\pi}\int_{-\infty}^{\infty} g_1(t)e^{-i\omega t}\,dt, \tag{1}$$

using the simplified Filon method on a logarithmic grid [38,39]. In that process, a straightforward calculation of $g_1(t)$ involves taking the square root of the measured intensity correlation function, and thus strongly enhances noise at long times, where the correlation function has almost decayed. To remedy this, we adopted the following procedure: One observes from Fig. 2(a) that the *long-time* part of the decay is well reproduced by a stretched exponential (KWW) function, $g_2(t) \approx a\exp[-(t/\tau)^\beta]$. Taking the square root, this transforms to the same function with amplitude $\sqrt{a}$, shifted on the time axis by a factor of $2^{1/\beta}$. Therefore, we replaced the noisy long-time values of the calculated $g_1(t) = \{[g_2(t) - 1]/\Lambda\}^{1/2}$ by rescaled values of $g_1^2(t)$ *in this long-time region*, with the scaling factors determined from a KWW fit to the data of $g_1^2(t)$. We emphasize that for this procedure to work it is not necessary that the entire $g_1^2(t)$ be reproduced by a stretched exponential fit, since only the long-time part of the decay is reconstructed by this procedure. The method is exemplified in Fig. 2: A KWW function is adjusted to the original $g_1^2(t)$ (circles) at long times (solid line), so that $g_1(t)$ can be calculated directly for short times ($t/\tau \lesssim 1$; squares) and obtained by the scaling procedure for long times ($t/\tau \gtrsim 1$; diamonds). The resulting

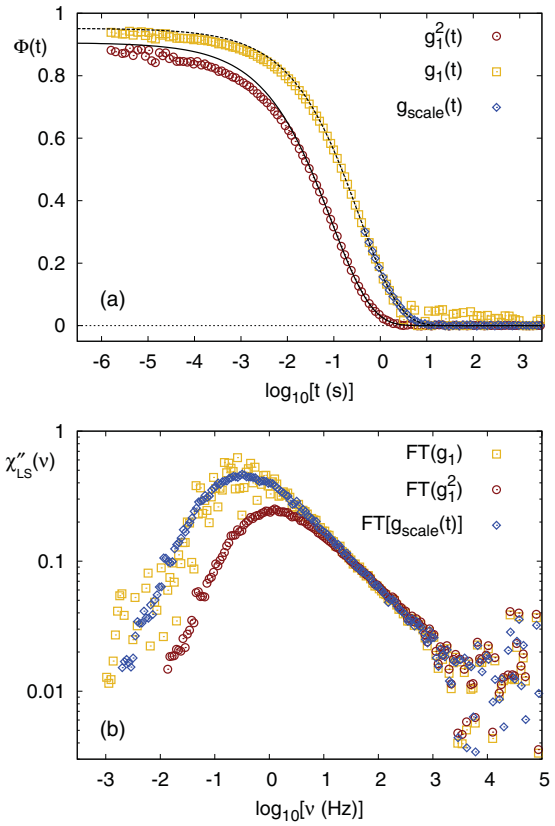

FIG. 2. (Color online) (a) Measured PCS correlation function $g_1^2(t)$ (circles) and its square root $g_1(t)$ (squares). To improve the signal-to-noise ratio at long times, $g_1(t)$ is obtained there by a scaling procedure from $g_1^2(t)$ that avoids taking the square root numerically (diamonds; see text for details). Black lines are fits to stretched exponential functions for $t \geqslant 0.1$ s. (b) Numerical Fourier transforms corresponding to the data in (a).

$g_1(t)$ is not necessarily a KWW function, as exhibited by the dashed line in Fig. 2(a). The validity of the approach is checked in Fig. 2(b) by considering the Fourier transform: The direct FT of $[g_1^2(t)]^{1/2}$ (squares) is compared with the one obtained by the scaling procedure (diamonds). Apart from the dramatic reduction in noise on the low-frequency side of the peak in the latter, the two transforms agree.

Having obtained the Fourier-transformed PCS spectra, we can compare with previous light-scattering results obtained with a Tandem-Fabry-Perot (TFP) setup, Ref. [37]. The result is shown in Fig. 3. Here we are faced with the need to consistently normalize both data sets. While for the TFP data of Ref. [37] the normalization could be determined independently, this was not possible in the present experiment, due to the very low scattering intensity of propylene carbonate. Thus, we make use of the sum rule [40]:

$$\int_0^\infty \chi''(\omega)\,d\ln\omega = \frac{\pi}{2}. \tag{2}$$

At $T = 165$ K, both PCS and TFP data exist, but the TFP data just cover the range down to the MCT β-minimum, $\omega \approx 0.1$ GHz, while our PCS data only allow a reliable Fourier transform up to $\omega \approx 1$ kHz. For the purpose of estimating the normalization, missing data in this gap were interpolated by

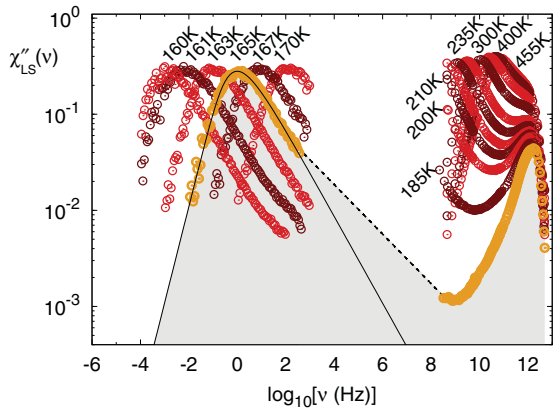

FIG. 3. (Color online) Susceptibility spectra $\chi''_{LS}(\nu)$ of propylene carbonate at different temperatures ($T = 160$, 161, 163, 165, 167, 170, 185, 200, 210, 220, 235, 300, 400, and 455 K) obtained from depolarized light scattering. Data above $\nu = 10^8$ Hz are from Tandem-Fabry-Perot measurements of Ref. [37]; low-frequency data are our PCS measurements. The dashed line indicates a simple interpolation between the two data sets for $T = 165$ K used to normalize the PCS data (see text). The solid line is a Cole-Davidson fit.

a trapezoidal rule indicated by a dashed line in Fig. 3. With this interpolation, Eq. (2) was be evaluated to determine the normalization factor needed for the raw PCS data. The same normalization has then been applied to the PCS data sets at the other temperatures.

Although the dashed line in Fig. 3 only represents a crude interpolation, it still suffices to point out that some additional relaxation modes likely exist on the high-frequency side of the measured α-peak. This is suggested by the enhancement of the dashed line over the phenomenological Cole-Davidson function (sold line) that is often used to describe stretched-exponential relaxation in the frequency domain. From dielectric spectroscopy measurements, such contributions are known either in the form of the slow β-mode or the excess wing, also in propylene carbonate [4,5,41]. Although the particular form of the relaxation spectra is known to differ among the two methods [42,43], we thus find evidence for an excess β-mode to also exist for propylene carbonate in light scattering. This contribution, however, appears to be rather small, in agreement with previous findings for salol, 2-picoline, and dimethyl phtalate [44], where the excess wing was consistently found to be stronger in dielectric spectra than in depolarized light scattering.

III. MODE-COUPLING THEORY

A. Hopping model

The mode-coupling theory of the glass transition (MCT) aims at capturing the slow dynamics induced by slow relaxation of density fluctuations in dense liquids [2,45,46]. It formulates a closed equation of motion for the density autocorrelation function $\Phi_q(t) = \langle \varrho^*(\vec{q},t)\varrho(\vec{q},0)\rangle$, where $\varrho(\vec{q},t) = \sum_k \exp[i\vec{q}\cdot\vec{r}_k(t)]/\sqrt{N}$ is the density fluctuation at wave vector $\vec{q}$ in a system of $k = 1,\ldots,N$ structureless, spherically symmetric particles with positions $\vec{r}_k(t)$. This function is in principle directly accessible, e.g., in neutron scattering, and is thought to indirectly also govern the autocorrelation functions measured in light scattering or dielectric spectroscopy [47,48]. The MCT equations are a set of nonlinear coupled integro-differential equations that completely determine the dynamics of $\Phi_q(t)$, given the static information. Essentially, the static structure factor $S(q)$ and similar equilibrium static correlation functions enter here. This allows for a first-principles comparison of the theory with simple glass-forming liquids, most prominently the hard-sphere system [49–52]. Details of the theory are found in Ref. [2].

Although the theory is readily extended to deal with nonspherical molecules [53–56], the resulting mathematical complexity typically hinders direct tests of the full MCT for the standard glass formers. One way to apply MCT beyond its asymptotic scaling laws in such cases is to employ so-called schematic models. Here, one single-handedly reduces the large set of coupled MCT equations to only a few, in practice just one or two. This often amounts to dropping the wave-vector dependence, although the true justification is that one reduces the model to the simplest one that falls into the same universality class of MCT glass transitions [2]. The resulting simplicity is paid for by the introduction of fit parameters that replace the microscopically derived connection between $S(q)$ and the theory's coupling vertices. On the other hand, adjusting these parameters as fit parameters often leads to a remarkable quantitative agreement with experimental data [23–25].

Turning an apparent weakness to a strength, schematic MCT models also provide a flexible testing ground for extensions of MCT. This was demonstrated for the inclusion of hopping processes earlier [27]. Extending the schematic MCT by a constant hopping term, susceptibility spectra of propylene carbonate from neutron scattering, light scattering, and dielectric spectroscopy could be fitted in the high-frequency regime, and an apparent violation of the MCT scaling laws could be explained by typical preasymptotic corrections [43]. To uncover these corrections to scaling, it is essential to consistently analyze spectra from multiple experimental methods.

Introducing the Laplace transform of the correlator,

$$\Phi(z) = i\int_0^\infty e^{izt}\Phi(t)\,dt, \tag{3}$$

we write the equation of motion for our schematic model as

$$\Phi(z) = -\left[z + \Delta(z) - \frac{\Omega^2}{z + i\nu + \Omega^2 m(z)}\right]^{-1}. \tag{4}$$

Equations of this form are common in a correlation-function description of the dynamics of a many-particle system, and are derived by using a projection-operator formalism introduced by Zwanzig and Mori [57]. Here, $m(z)$ is a memory kernel of fluctuating forces that is the core target of MCT's approximations. Ω^2 and ν are constants taken to reflect the microscopic short-time motion; neglecting $\Delta(z)$ and $m(z)$ completely results in a damped harmonic-oscillator equation for $\Phi(z)$ that mimics the peak visible in the THz regime of Fig. 3. This description of the Raman band is not accurate at all, but we shall be concerned with the low-frequency respectively long-time behavior of the correlation functions only.

The original schematic MCT is obtained by setting $\Delta(z) \equiv 0$ and approximating the memory kernel $m(z)$ as a nonlinear functional of the correlator in the time domain, $m(t) = \mathcal{F}[\Phi(t)]$. The simplest schematic MCT model that allows one to reproduce the whole range of asymptotic power laws predicted by the microscopic theory is the F_{12} model, specified by

$$m(t) = v_1\Phi(t) + v_2\Phi(t)^2. \tag{5}$$

Here, v_1 and v_2 are coupling coefficients that encode the molecular interactions and are assumed to be smoothly increasing functions of external control parameters such as density, pressure, or inverse temperature. The appearance of a quadratic term in Eq. (5) is essential; it gives rise to bifurcations in the long-time limits of the correlators, $f = \lim_{t\to\infty}\Phi(t)$, identified as the idealized-MCT glass transition. Although the coupling coefficients change smoothly, at critical values along a line (v_1^c, v_2^c), f jumps discontinuously from zero to a finite value f^c—the solutions of the model become nonergodic in this idealized glass state. Apart from special higher-order singularities, there is an exponent parameter $\lambda \in [1/2, 1[$ associated to every transition point, that determines nonuniversal power-law exponents a and b governing the long-time dynamics asymptotically close to the transition. Specifically for the F_{12} model one has $v_1^c = (2\lambda - 1)/\lambda^2$, and $v_2^c = 1/\lambda^2$. The transition gives rise to the celebrated two-step decay scenario for $\Phi(t)$, with an initial decay asymptote $\Phi(t) \sim f^c + h(t/t_0)^{-a}$ toward a plateau given asymptotically by f^c, and a von Schweidler decay $\Phi(t) \sim f^c - h'(t/t_\sigma)^{-b}$ from the plateau toward zero on the liquid side of the transition. Here, t_0 is a time scale characteristic of the short-time motion, implicitly set by Ω^2 and ν; t_σ is a time scale that diverges upon approaching the transition. In the frequency domain, the two asymptotes translate to the low- and high-frequency power laws around the β-minimum mentioned above. The approach to the idealized MCT transition at (v_1^c, v_2^c) from the liquid side is accompanied by a second divergent relaxation time in $\Phi(t)$, the α-relaxation time that governs the long-time decay of the correlation functions.

The central idea of schematic extended-MCT models is to incorporate additional relaxation processes not captured in the spirit of Eq. (5), that restore ergodicity even in the idealized glass state. Recall that in this case $\Phi(z) \sim -f/z$ for $z + i0 \to 0$ is implied by $f > 0$ through Eq. (3), so that for $\Delta(z) \equiv 0$ the last term in the brackets of Eq. (4) needs to become arbitrarily small in order to support a nonergodic solution. This is indeed guaranteed by Eq. (5) since with $\lim_{t\to\infty}\Phi(t) = f$ then also $m(z) \sim -m[f]/z$ from Eq. (3). It is also easily seen that any finite $\Delta(z)$ will make the solution ergodic again. Physically, Eq. (4) expresses a parallel relaxation scheme: The last term encodes the cage effect described by MCT, a relaxation channel that is effectively closed in the glass. $\Delta(z)$ on the other hand describes a second slow relaxation channel that presumably, due to it being a small correction to the cage effect relaxation, can be dropped in a first approximation as long as the cage relaxation is not completely arrested—this is the idealized MCT. If the primary MCT relaxation channel however vanishes, any nonzero contribution to $\Delta(z)$, however small, will dominate the solutions at long times and thus needs to be taken into account.

Transforming Eq. (4) into the time domain, one gets

$$\begin{aligned}\ddot{\Phi}(t) + (\Delta * \dot{\Phi})(t) + [\Delta(t) + \dot{\Phi}_0\delta(t)] + \nu\dot{\Phi}(t) \\ + \nu(\Delta * \Phi)(t) + \Omega^2\Phi(t) + \Omega^2(m * \dot{\Phi})(t) \\ + (\Delta * m * \Phi)(t) = 0.\end{aligned} \tag{6}$$

Here, we have abbreviated the convolution of two functions $f(t)$ and $g(t)$ by $(f * g)(t) = \int_0^t f(t-\tau)g(\tau)\,d\tau$. Equation (6) has to be solved with the initial conditions $\Phi(0) = 1$ and $\partial_t\Phi(t)|_{t\to 0} = \dot{\Phi}_0 = -\Delta(0)$. Approximating $\Delta(t) \approx \delta_0\delta(t)$ as a Markovian rate, i.e., $\Delta(z) \approx i\delta_0$, leads to the extended-MCT model studied before [21,27], also in the context of wave-number-dependent correlators [29]. Equation (6) holds for systems governed by Newton's equations of motion. On the other hand, for colloidal suspensions an overdamped dynamics can be formulated. Note that the results we discuss below for long times (low frequencies) are not affected by such a change. This is in line with findings that both the cage effect and hopping-induced motion are universal among both system classes [58].

Clearly, the time dependence of $\Delta(t)$ is of importance if one wants to describe the nonexponentiality of the relaxation below T_c. For a time scale $t \gg t_\sigma$ and in the absence of $\Delta(z)$, the cage-effect channel in Eq. (4) has already attained its long-time limit; i. e., $m(z \to 0) \sim -m[f]/z$ with $m[f] = f/(1-f)$ [59]. Inserting this into Eq. (4), we obtain $\Phi(z) = -1/[z/f + \Delta(z)]$, or in the time domain,

$$\dot{\Phi}(t) = -f\int_0^t \Delta(t-t')\Phi(t')\,dt' \tag{7}$$

with initial condition $\Phi(t) = f$. Of course, this approximation neglects the effect of $\Delta(z)$ on the memory kernel via Eq. (5) and thus does not capture the exact long-time behavior of Eq. (6). However, it was recognized earlier [60,61] that *any* empirical distribution of relaxation times, such as that for a stretched exponential relaxation $\Phi(t) \propto \exp[-(t/\tau)^\beta]$, can be written in the form of Eq. (7) if one admits the generalization

$$\Delta(t-t') \approx \Delta(t,t') \approx \hat{\Delta}(t')\delta(t-t'), \tag{8}$$

so that $\Phi(t) \sim f\exp[-R(t)]$ where $R(t) = \int_0^t f\hat{\Delta}(t')dt'$. Equation (8) has to be understood as an approximation valid for intermediate and long times only. It apparently violates time-translational invariance and, like many of the commonly applied phenomenological model functions such as the stretched exponential function, is not expected to be correct for $t \to 0$. Thus, it should be applied on mesoscopic timescales only. One may envisage the relaxation to be composed of random events that have a nonuniform rate $\Delta(t)$, which in turn may be a useful approximation to model dynamic heterogeneity [61] and intermittent relaxation. The interpretation to describe the relaxation of density fluctuations as a random process of the form $\Phi(t) = E\{\exp[-H(t,\omega)]\}$ (where $E\{\cdot\}$ denotes the expectation value and ω is a random variable), i.e., exponential relaxations with random local time H, has been suggested by Sjögren [62] to be central to MCT. The connection of Eq. (8) to Feller's theory of renewal processes [63] has been pointed out previously [61]. We hence conclude that Eq. (8) allows one to capture the physics of dynamically heterogeneous activated dynamics, in line with the common interpretation of dynamics below T_c.

Inserting the approximation (8) into Eq. (6) leads to a significant simplification of the latter, as many of the convolutions drop out:

$$\ddot{\Phi}(t) + [(\nu + \hat{\Delta}(t)]\dot{\Phi}(t) + [\Omega^2 + \nu\hat{\Delta}(t)]\Phi(t) + \Omega^2(m * \dot{\Phi})(t) + \Omega^2\hat{\Delta}(t)(m * \Phi)(t) = 0. \quad (9)$$

The convolution-less appearance of memory kernels in the equations of motion for correlation functions can be derived formally using modified projection operators introduced by Mori and Tokuyama (MT) [64]. These authors have argued that such a route is better suited than the Zwanzig-Mori projection scheme used to derive Eq. (4) to address random frequency variations in stochastic oscillators and related problems. A description of glassy dynamics on the basis of this MT scheme has been suggested [65]. But note a crucial difference to our Eq. (9): Here, we still rely on the retarded friction kernel m as suggested by MCT to provide the essential features of glassy dynamics, in stark contrast to Ref. [65]. But consistent with the interpretation of Ref. [64], we model the hopping contribution $\hat{\Delta}$ in a way that could conceivably be derived within the MT projection scheme.

Clearly, in a single-correlator model the time dependence of $\hat{\Delta}(t)$ is responsible for the stretching of the hopping-induced relaxation, while its overall magnitude controls the relaxation time scale. For the former, an MCT-inspired ansatz suggests a polynomial in $\Phi(t)$. For the latter, Chong [29] has recently suggested a simple semiempirical model: Assuming localized hopping events that are embedded in the glassy structure, one derives a rate that is given by an Arrhenius form where the strength of the frozen matrix—its elastic modulus—enters the effective barrier height for the activated events. The longitudinal elastic modulus exhibits a thermodynamic contribution that varies smoothly across the MCT transition, and a nonergodic contribution essentially given by the MCT memory kernel $m(t \to \infty) = m[f]$ [66], that arises in the glass only. In the schematic model, we set

$$\tilde{f}\,\hat{\Delta}(t) \approx \Phi(t)^2\, e^{-Mm[\tilde{f}]/(\varrho\, k_B T)}, \quad (10)$$

where $\tilde{f} = f$ in the glass, and $\tilde{f} = f^c$ in the liquid. Here, M represents the longitudinal elastic modulus and ϱ and k_B are the number density and Boltzmann constant, respectively. In the following we set $M/(\varrho\, k_B T) \approx 50$ as a typical value of elastic moduli in dense liquids whose interactions are dominated by hard-core repulsion [66]. We note here that smaller values of M will enhance the hopping contribution and that $m[f]$ increases as one enters deeper into the glass. Let us also stress that the precise form of the Arrhenius factor in Eq. (10) is not essential for our discussion. One could equally try to estimate these hopping rates based on different approaches [67]. The quadratic dependence of $\hat{\Delta}(t)$ on $\Phi(t)$ could be replaced by a linear one as suggested by Greenall and Cates [33], in a slightly different context, to be more appropriate for intermittent hopping relaxation. This would result in somewhat less stretching of the final relaxation, but would not change our results qualitatively. Ultimately, the correct form cannot be decided within a schematic model.

Numerical results for the schematic model with memory kernel Eq. (5), and hopping kernel specified by Eqs. (8) and (10), are shown in Fig. 4. Here, the critical point corresponding

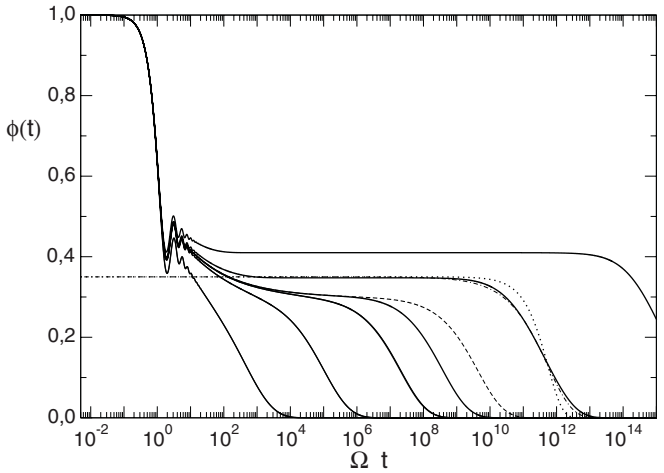

FIG. 4. Schematic F12-model correlators $\Phi(t)$ with hopping kernel according to Eqs. (8) and (10). Parameters $(v_1, v_2) = [v_1^c, v_2^c(1 + \varepsilon)]$ with $\varepsilon = -0.1$, -0.01, -0.001, -0.0001, 0.01, and 0.05, from left to right. (v_1^c, v_2^c) are fixed according to $\lambda = 0.7$ (see text). A dashed line shows the solution without hopping term for $\varepsilon = -0.0001$. The dash-dotted line is a stretched exponential function, $f \exp[-(t/\tau)^\beta]$ with $\beta = 0.6$; the dotted line shows pure exponential relaxation for comparison.

to an exponent parameter $\lambda = 0.7$ has been selected. State points close to this critical point are then chosen according to $v_1 = v_1^c$ and $v_2 = v_2^c(1 + \varepsilon)$. Hence, $\varepsilon < 0$ corresponds to liquid states, and $\varepsilon > 0$ to states in the idealized-MCT glass.

Sufficiently far from the critical point on the liquid side, the solutions with and without hopping kernel coincide; for the parameters chosen, this holds up to $\varepsilon = -0.001$. As noted in Ref. [27], even a hopping rate that increases with an Arrhenius law—as expected for thermally activated processes—is eventually dominated by the cage effect, given a sufficiently low activation energy. This justifies the use of idealized MCT for those liquid states. Close to the transition, the relaxation is enhanced by hopping, as exemplified for $\varepsilon = -0.0001$ in Fig. 4, where a dashed line indicates the corresponding idealized-MCT result, $\Delta(t) \equiv 0$. In the present model, this simply amounts to a shift in the final relaxation time, essentially without a change in shape. Hence, the idealized-MCT divergence of relaxation times is cut off, and the transition "avoided".

In the ideal glass, $\varepsilon > 0$, Fig. 4 shows the hopping-induced decay of the correlation function. This is still nonexponential, as shown by comparison with a pure exponential (dotted line). Indeed a stretched-exponential curve (dash-dotted) with stretching parameter $\beta = 0.6$ provides a reasonable fit for $\varepsilon = 0.01$. For the specific model here, the stretching is very similar to the one also found on the liquid side of the transition. However, the original glass-transition singularity is still evident, since for $\varepsilon > 0$, the plateau value rises asymptotically as $f \sim f^c + h\sqrt{\varepsilon}$, where h is a constant critical amplitude. In the liquid, one has $f \sim f^c$ asymptotically (up to corrections that are linear in ε), so that the point $\varepsilon = 0$ can in principle be identified as the position of a square-root singularity. This was demonstrated experimentally by various methods for a number of commonly studied glass-forming liquids [7–16].

The scenario of Fig. 4 also qualitatively explains recent findings for hard-sphere-like colloids [68].

B. Probe-correlator model

We now discuss the dynamics of probe-density fluctuations that are measured by a given spectroscopic technique in lieu of the underlying collective dynamics of the system which is described by the extended F_{12}-model correlator.

Following Sjögren [69], the coupling is most simply expressed by writing an analog of Eq. (4) for a second correlator $\Phi_A^s(z)$, expressing the fluctuations of a dynamical variable A that is probed in experiment. This could be the reorientation of permanent dipoles or a polarizability tensor or describe the q-dependent coupling of incoherent scattering to the collective density fluctuations in neutron scattering [26,27]. In particular, the Laplace transform of the correlator determines the dynamic susceptibility of the probe variable A:

$$\chi_A(z)/\chi_A = z\Phi_A^s(z) + 1, \tag{11}$$

where χ_A is the thermodynamic susceptibility. We will in the following mainly discuss the normalized susceptibility spectra, $\chi_A''(\omega)/\chi_A = \omega\Im\Phi_A^s(\omega)$, connected to the imaginary part of the Laplace-transformed correlator for real frequencies $\omega = z + i0$. We are not intending a theory of thermodynamic features, so χ_A is treated as an adjustable parameter, temperature independent for the sake of simplicity.

The memory kernel $m_A^s(z)$ appearing in the analog of Eq. (4) is then written as

$$m_A^s(t) = v_A^s\,\Phi(t)\Phi_A^s(t). \tag{12}$$

In the following, we will analyze dynamic light scattering data, $A = \mathrm{LS}$, and dielectric spectroscopy data, $A = \mathrm{DS}$.

We make use of the fact that hopping motion will be present both for the collective density correlator $\Phi(t)$, and for the probe correlator $\Phi_A^s(t)$. To simply model the decay to an ergodic state, a hopping term for the former would suffice, due to the linear coupling expressed in Eq. (12). But as we will see below, the intricate shape of the combined α- and slow β-relaxations are better modeled by taking both terms into account.

As an example, consider the obvious generalization of Eq. (10):

$$\tilde{f}^s\,\hat{\Delta}^s(t) \approx \Phi(t)\Phi_A^s(t)\,e^{-Mm[\tilde{f}]/(\varrho\,k_BT)}, \tag{13}$$

where we have assumed that the time dependence is governed by probe-density correlations, and that the escape rate even of the single particle is still given by the collective rate (modulo a static structure factor as a prefactor [29], which is unity here). The appearance of $\Phi(t)$ in Eq. (13) embodies the fact that hopping relaxation in glass formers is a highly collective effect, as seen in the absence of an isotope effect in tracer diffusion in metallic glass formers both above and below T_c [70].

Figure 5 shows the dynamic susceptibilities $\chi''(\omega)$ calculated from the correlators $\Phi(t)$ and $\Phi_A^s(t)$ in the model thus defined. For this example, we have set $v_A^s = 50$, a value that is of the typical magnitude fitted to experimental data (see below). Turning first to the spectra of the collective correlator $\Phi(t)$ (top panel), one again clearly identifies the features of nonexponential relaxation even inside the ideal-glass state. A comparison with a Debye-relaxation function,

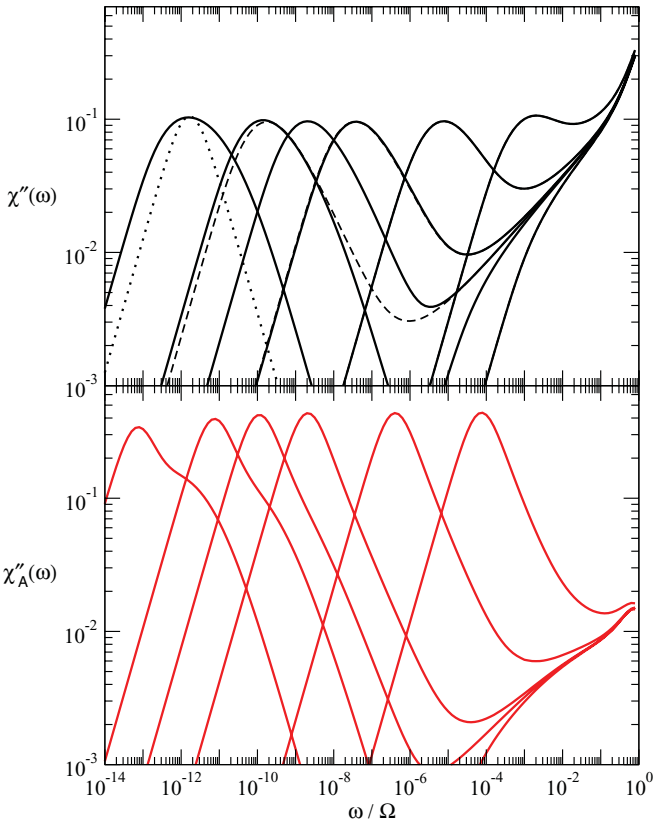

FIG. 5. (Color online) Dynamic susceptibilities calculated from the schematic Sjögren model with hopping terms according to Eqs. (10) and (13); $v_A^s = 50$. Top panel: $\chi''(\omega)$ corresponding the collective correlations $\Phi(t)$. Bottom panel: $\chi_A''(\omega)$ corresponding to the probe-variable fluctuations. Parameters as in Fig. (4); distance parameters shown are $\varepsilon = -0.1$, -0.01, -0.001, -0.0001, 0.001, and 0.01. For $\chi''(\omega)$, the result for $\varepsilon = -0.0001$ without hopping term is shown as a dashed line. The dotted line is a Debye function for reference.

$\chi''_{\mathrm{Debye}}(\omega) \propto \omega\tau/[1 + (\omega\tau)^2]$, shown in dotted, reveals this. Shown in dashed is a spectrum without hopping term close to the transition on the liquid side. Comparing with the results including hopping, one finds that the stretching almost stays constant as one crosses the glass transition.

The susceptibility spectra (lower panel of Fig. 5) follow the same qualitative trend. As typically found [27], the stretching for $\chi_A''(\omega)$ is less, and the strength of the α-relaxation peak is simultaneously enhanced for the choice of large coupling strength v_s. For the state points farthest into the glass, one notices the splitting of the relaxation peak into two contributions. This is a result from the coupling between $\Phi_A^s(t)$ and $\Phi(t)$ in the model. The relaxation of $\Phi(t)$ induces relaxation in $\Phi_A^s(t)$, but on the same time scale, the slightly slower hopping term constitutes a second relaxation mode; thus, two time scales can be identified in the decay of $\Phi_A^s(t)$. The shorter time scale corresponds to the decay of collective fluctuations, and induces a shoulder in the high-frequency flank of the α-relaxation peak in $\chi_A''(\omega)$. This shoulder bears some reminiscence of a slow β-peak that emerges as one moves deeper into the idealized-glass state.

C. Model with Kohlrausch relaxation rates

So far, the schematic Sjögren model with *ad hoc* time-dependent hopping rates has been presented as an example of how to generate stretched decay inside the MCT glass state, and how density and probe correlators can conspire to yield a feature akin to a slow β-peak in the presence of two distinct hopping-rate kernels. The model, however, has some drawbacks that do not allow us to fit it to experimental data: The broadening of the spectra, in particular in the β-peak (or HF-wing) region, is much less than observed. We attribute this to the assumed form of the hopping rate, $\hat{\Delta}(t) \sim \Phi(t)^2$, being still too narrow. A particular consequence is the appearance of a deep minimum in the spectra for $T < T_c$ that is not consistent with experimental data [71].

To show that the interpretation of the slow β-modes as the interplay between collective relaxation and probe-variable relaxation is still consistent within the extended MCT, we thus return to the generalized hopping rate Eq. (8) and set

$$\hat{\Delta}_{\mathrm{KWW}}(t) = \beta \frac{t^{\beta-1}}{f\tau^{\beta}} \tag{14}$$

to obtain a stretched exponential relaxation as solution of Eq. (7). Although the stretched-exponential relaxation for long times is only an empirical description going back to Kohlrausch [72], the original MCT is in a certain limit compatible with such a limiting form of the correlation functions [73]. Note that $\hat{\Delta}_{\mathrm{KWW}}(t)$ diverges as $t \to 0$, since the stretched-exponential relaxation has no regular short-time expansion. To make the model well defined, we regularize this rate and set in Eq. (9)

$$\hat{\Delta}(t) = \begin{cases} \hat{\Delta}_{\mathrm{KWW}}(1/\Omega), & t < 1/\Omega, \\ \hat{\Delta}_{\mathrm{KWW}}(t), & t \geqslant 1/\Omega, \end{cases} \tag{15}$$

which seems reasonable as the model is only intended to be applied for times larger than the time scale of microscopic motion set by $1/\Omega$. A corresponding expression is used for the probe correlator.

In summary, our model introduces the following set of fit parameters: (Ω, v) and (Ω_A^s, v_A^s) are used to model the microscopic dynamics and to fix the units of frequency and energy. The dependence of the low-frequency part of the solutions on these parameters is negligible, up to a rescaling of frequencies. (v_1, v_2) from Eq. (5) are the crucial control parameters driving the collective correlator $\Phi(t)$ through its idealized glass transition. v_A^s determines the strength for the coupling between probe and collective motion via Eq. (12); it must not be chosen too small in order for the probe to become arrested when the host liquid does [69]. Finally, there remain the hopping parameters, (τ, β) and (τ_A^s, β_A^s). They explicitly determine the shape of the α-relaxation below T_c, and are hence crucial in fitting this part of the data. No predictive power can be assigned to these fit parameters, as they are merely a more flexible way to adapt the shape of the relaxation peaks. However, once the hopping in the collective density fluctuations is fixed by (τ, β) this will subsequently affect the hopping terms in all individual probe correlators.

The simple Sjögren model, in which one determines the hopping rates from $\Phi(t)$ and $\Phi_A^s(t)$ directly, as proposed in the previous section, has a number of inherent limitations that are artifacts of the restriction to only two relevant correlators. For example, one finds for $T > T_c$ a strict connection between the α-peak height and its stretching, which is not present in the full theory, although its trend is sufficiently close to reality to make fits viable in the first place. However, a fit of real-world experimental data covering up to 18 orders of magnitude is a rather demanding test of any model, so that we levy the artificial, model-built restrictions by using Eq. (15) for $\Phi(t)$ and its analog for $\Phi_A^s(t)$. The emphasis will then be on the subtle interplay between these two hopping processes stipulated by Eq. (12) that is unique to the MCT ansatz. The possibility to consistently fit two different data sets, $A = \mathrm{LS}$ and $A = \mathrm{DS}$, using the same parameter set for the underlying $\Phi(t)$, is thus a nontrivial conclusion that can be drawn from our model.

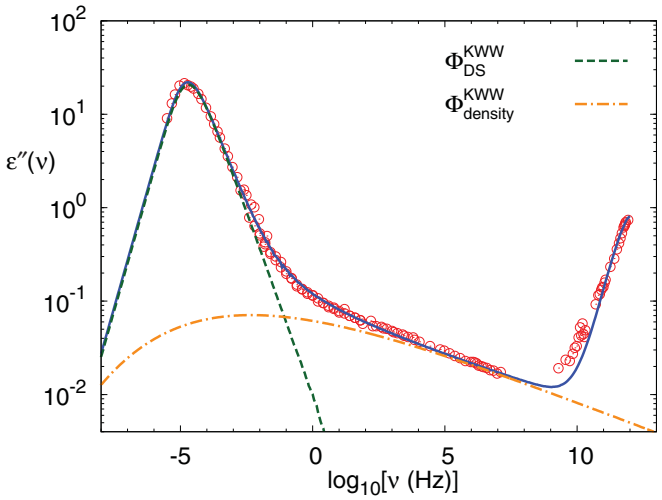

FIG. 6. (Color online) Fit of dielectric spectroscopy data for propylene carbonate at $T = 157$ K (symbols; from Ref. [74]) with the extended schematic-MCT model incorporating KWW-like hopping rates outlined in the text (solid line). The hopping contributions stemming from the collective correlator $\Phi(t)$ and from the probe-variable correlator $\Phi_{\mathrm{DS}}^s(t)$ are indicated separately (dashed and dash-dotted lines).

An example for the interplay between $\Phi(t)$ and $\Phi_A^s(t)$ is given in Fig. 6. Here we show dielectric relaxation spectra $\chi''_{\mathrm{DS}}(\omega)$ for $T = 157$ K from Ref. [74], far below T_c. The solid line interpolating the data symbols is the fit using the extended schematic model. Additionally, we have depicted both hopping contributions separately by making use of the approximations (7) and (8). Their relaxation times τ and τ_{DS}^s and stretching indices β and β_{DS}^s were chosen differently; as a result, the hopping contribution from the collective density correlator contributes a rather flat and extremely stretched background that serves to capture the excess wing contribution in the range $1\ \mathrm{Hz} \lesssim \nu \lesssim 0.1\ \mathrm{GHz}$. The α-peak properties are then determined by the hopping term chosen for the probe relaxation. Thus, by choosing the hopping parameters for the collective density fluctuations, the fits for different probe variables will not be independent any more, even in the region below T_c.

IV. DATA ANALYSIS

Fits of the schematic model to propylene carbonate data are shown in Fig. 7. The model outlined above turns out to provide

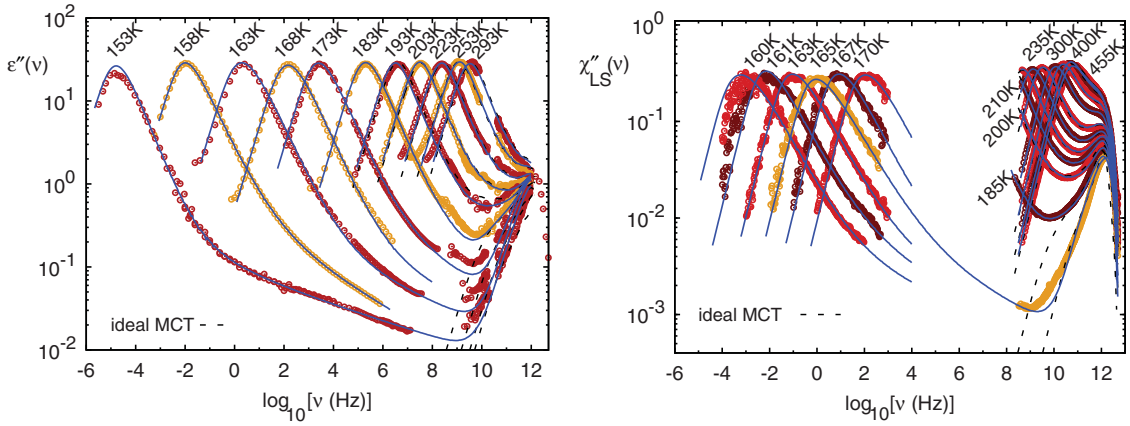

FIG. 7. (Color online) Susceptibility spectra for propylene carbonate as measured by dielectric loss spectroscopy (left; data from Ref. [74]), and by deploarized light scattering (right; data from Ref. [37] above 10^8 Hz; own measurements below 10^4 Hz); temperatures as indicated. Solid lines are fits with the extended schematic-MCT model. Dashed lines are fits with the ideal MCT model, i. e., without hopping term for comparison.

a consistent fit for both the combined PCS and Brillouin-scattering data set shown in Fig. 3 (Ref. [37] and our data), and the dielectric-spectroscopy data by Lunkenheimer *et al.* [74]. To achieve the quality of the fit visible in Fig. 7, we varied all fit parameters smoothly with temperature in a controlled way that reflects their physical meaning, as we shall describe below. With this procedure, the model gives an accurate account of all available data spanning up to 18 orders of magnitude in frequency, and 3 orders of magnitude in amplitude variation, for temperatures from around the melting temperature, down to below T_g.

The fit is consistent because it describes both data sets as originating from the *same* underlying model of collective dynamics $\Phi(t)$. In other words, for LS and DS data at the same temperature, the fit parameters entering $\Phi(t)$ were fixed simultaneously; only the fit parameters entering the respective $\Phi^s_A(t)$ were allowed to differ. In particular, the microscopic-relaxation parameters entering $\Phi(t)$ were fixed temperature-independently as $(\Omega,\nu) = (10,0)$ THz. For the dynamics above T_c, the coupling coefficients entering the memory kernel, v_1 and v_2, were then determined. Specifically, at T_c, the critical coupling coefficients (v_1^c, v_2^c) were chosen in agreement with the known asymptotic behavior close to the MCT transition. Earlier analyses [21,27,43,75] gave values between $\lambda = 0.72$ and 0.78; iterative refinement of the fits here resulted in $\lambda \approx 0.75$ at $T_c \approx 187$ K.

Having fixed this point along the glass-transition line, one imposes that $v_1(T)$ and $v_2(T)$ should be increasing functions of decreasing temperature, to express the increased coupling strengths as the liquid is further cooled. Here, we adopted the procedure of Ref. [27], demanding that the values follow a smooth path in the (v_1, v_2) parameter space of the model, and that their distance to the critical point is a linear function of the temperature difference to T_c. This is expressed by demanding that the separation parameter $\sigma = \lambda[(v_1 - v_1^c)(1-\lambda) + (v_2 - v_2^c)(1-\lambda^2)]$ derived from an asymptotic analysis of the model equations [2] is a linear function of T close to T_c. It ensures that the nontrivial variation of τ_α above T_c is a feature of the model, and not of the variation of the fit parameters. Initially, a prescribed smooth curve for $(v_1(T), v_2(T))$ was imposed; free fits with these starting values in a second step lead to only slight deviations. The variation of v_1 and v_2 is shown in Fig. 8 both directly in the (v_1, v_2) parameter space (inset), and in a representation that allows us to check the linear dependence $\sigma \sim (T_c - T)$. In this figure, independent results for the DS and LS data are shown; we demand them to lie on the same path. This is fulfilled with good accuracy, proving the consistency of the fits.

Next, the MCT parameters for the probe correlators $\Phi^s_{\mathrm{LS}}(t)$ and $\Phi^s_{\mathrm{DS}}(t)$ are adjusted. Ω^s_A and ν^s_A were allowed to vary smoothly with temperature [76], but this procedure only serves to give a satisfactory fit of the THz frequency regime. No physical significance can be further attached to these parameters since they are only representatives for what in

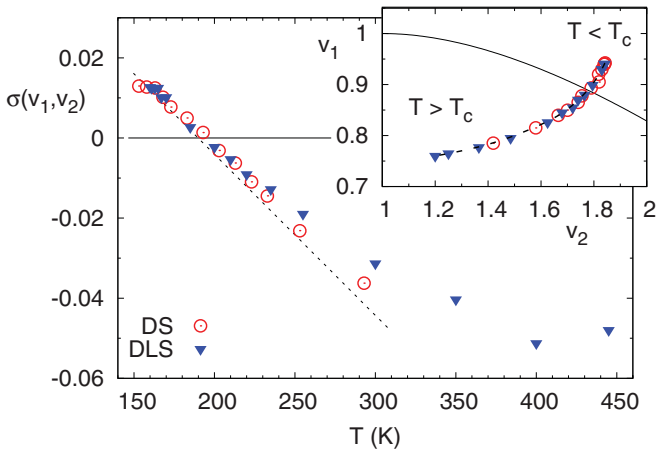

FIG. 8. (Color online) The separation parameter $\sigma(v_1, v_2)$ used in the fits of Fig. 7 as a function of temperature; a dotted line indicates the expected linear relation $\sigma \sim (T_c - T)/T_c$ close to T_c, and $\sigma = 0$ identifies the critical temperature $T_c \approx 187$ K. Independent fit results from analysis of the light-scattering (triangles) and dielectric-loss data (circles) are shown. The inset shows the fit parameters v_1 and v_2 in the parameter space of the model; the solid line indicates the line of glass transitions in the F_{12} model.

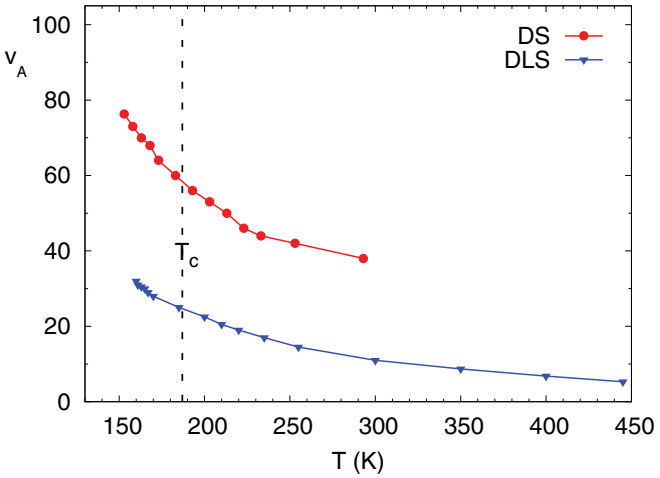

FIG. 9. (Color online) Coupling coefficients v_A^s describing the strength of probe-dynamics coupling to collective density dynamics in Eq. (12). Triangles show results for $A = \mathrm{LS}$, diamonds for $A = \mathrm{DS}$. The dashed line represents T_c.

reality is a superposition of wave-number dependent oscillator contributions.

More interesting are the coupling strengths entering the memory kernel Eq. (12), v_A^s. These are shown for the dielectric, $A = \mathrm{DS}$, and the light-scattering, $A = \mathrm{LS}$, data in Fig. 9. Again, both parameters are smoothly increasing functions of decreasing temperature. As discussed earlier [27], the coupling v_{DS}^s for the dielectric probe to the collective density dynamics is significantly stronger than that for v_{LS}^s. This is expected on grounds of the different rotational contributions probed by the two techniques: Dielectric spectroscopy is sensitive to dipole relaxations related to the Legendre polynomial of degree $\ell = 1$, while depolarized light scattering has several possible microscopic origins connected to $\ell = 2$. Generically, the coupling strengths decrease with increasing ℓ [42]. Note that the v_A^s also determine, below T_c, the appearance of the excess wing relative to the α-peak. This means that a consistent description of the wing in both data sets by our model is a nontrivial result. It should however be noted that the large gap in the accessible frequency window for the light-scattering techniques does not allow us to draw a final conclusion regarding this aspect of the model.

Below T_c, the hopping parameters τ and β are decisive. Again, we demand that the parameters entering $\Phi(t)$ agree for both data sets. This is again confirmed by independent fits, as shown in Fig. 10 (triangle symbols). The parameter β is found to decrease with decreasing temperature, and becomes very small around T_g, reflecting the broadness of the excess wing or slow β-peak. At the same time, the stretching parameters β_A^s entering the probe correlators are only weakly temperature dependent reflecting the approximate validity of the time temperature superposition principle. For $A = \mathrm{LS}$, the values of β_A^s are lower, which reproduces the known correlation between α-peak strength and stretching [27,42].

The hopping time scales are shown in the lower panel of Fig. 10. The fit procedure yields that these cannot be modeled by simple Arrhenius behavior. This is consistent with the expression equivalent to Eq. (10) obtained by

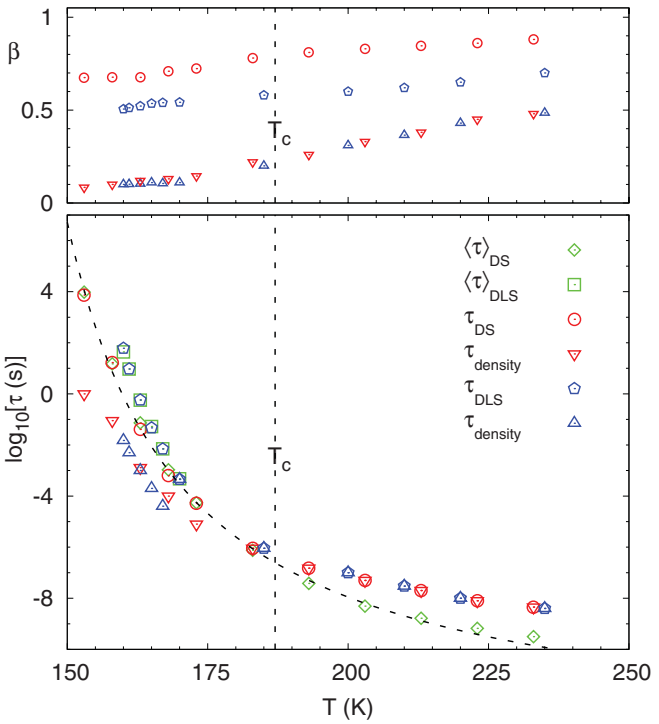

FIG. 10. (Color online) Hopping model parameters τ (lower panel) and β (upper panel) entering the collective density correlator $\Phi(t)$ (triangles) and the observable-specific correlators $\Phi_A^s(t)$ (circles for $A = \mathrm{DS}$; pentagons for $A = \mathrm{LS}$). For comparison, the mean relaxation time $\langle\tau\rangle_A$ determined from KWW fits to the experimental data are shown.

Chong *et al.* [29,30], where hopping is incorporated into MCT by the dynamical theory for diffusion-jump processes. In this framework the plateau height enters the expression for the hopping rates, in particular the activation energy. As this plateau height is temperature independent above T_c and follows the square-root dependence below, an extra temperature dependence of the activation energy is generated, which leads to a crossover from a rather weak temperature dependence of the hopping rates and $\tau_{\mathrm{hop}} > \tau_{\mathrm{MCT}}$ above T_c to a high activation energy of the hopping times below the critical temperature [30].

V. SUMMARY AND CONCLUSIONS

We have presented an *ad hoc* generalization of schematic models of the mode-coupling theory of the glass transition, to describe the stretched-exponential relaxation due to hopping effects in deeply supercooled liquids close to T_g. The model describes hopping motion as an intermittent stochastic process that can be viewed as a superposition of individual cage-escape events due to density fluctuations, occurring with a time-dependent rate distribution. While not justified by a complete microscopic derivation along the lines applied for the original MCT, this model incorporates ideas from both the original MCT literature as well from descriptions more amenable to activated events in amorphous solids.

In the simplest self-consistent approximation for the hopping rate, our model already gives rise to stretched-exponential decay in the glass, with stretching exponents close to those

observed on the liquid side of the transition. For probe-variable fluctuations, the susceptibility spectra show α-relaxation peaks that develop a shoulder on their high-frequency side reminiscent of the slow β-peak found in many glass formers. This can be achieved by adopting an activation barrier for the hopping rates that depends on the elastic properties of the medium, similar to the one recently proposed by Chong [29], which for our model introduces only one additional globally adjustable parameter. The model then serves to highlight the possible interplay of collective and probe-density fluctuations below T_c. In its simplistic form put forward above, it is, however, not directly applicable to describe experimental data.

Spectra from dielectric spectroscopy and light scattering can be fitted over up to 18 decades in frequency, covering a temperature range including T_g, T_c, and T_m, if, instead, one applies a more empirical ansatz for the hopping rate. We show that the emergence of nontrivial high-frequency features of the α-relaxation peak that are consistent with both measurements can indeed be well described by the model. Data from further techniques, such as mechanical spectroscopy, would be needed to make the test of the model even more stringent; our present fits then already fix a number of fit parameters for such a test.

Our model assigns two different mechanisms to the two prominent features of the low-frequency dynamics below T_c: The α-peak is described as a hopping-induced relaxation of the probe motion itself, which differs in strength, shape, and position among the measurement techniques, because these techniques couple to different probe variables. The slow β-excess wing, on the other hand, is assigned to the hopping-induced sub-T_c motion of the collective density matrix, which on its own is not accessible in either dielectric spectroscopy or light scattering.

If true, several consequences arise: The β-peak/excess wing should in first approximation have a similar position and width/slope independent of the measurement technique. The process can in principle appear as a wing, or as a separate slow β-relaxation peak, depending on the position, strength, and shape of the α-relaxation that is dominated by the probe-variable dynamics. And indeed, it has been noted that the excess wing shows a high degree of universality in many systems [77]. We also note that our model is fully consistent with the idea that both excess wing and β-peak, which previously were used to distinguish two types of glass formers [78], have in fact the same underlying mechanism [4,5]. Of course, the slow Johari-Goldstein β-relaxation, to which the excess wing can most probably be assigned [79], is thought to involve intermolecular degrees of freedom [80]. However, depending on the particular molecular structure, secondary processes also occur due to intramolecular motion in nonrigid molecules. But even in the latter case the present model would still be valid, as long as collective fluctuations are involved in the observed secondary process.

As one approaches T_c from below, the hopping-induced motion eventually is dominated by the idealized-MCT cage effect. Here, a strong coupling of the different dynamical variables and the vicinity of a bifurcation critical point (at T_c) imply that the difference between α- and slow β-relaxation vanishes; only a single α-peak survives above T_c. This is consistent with the finding in many glass-forming systems that the high-frequency wing contribution tends to vanish at a temperature around T_c upon heating [77].

ACKNOWLEDGMENTS

Th.B. gratefully acknowledges support by the Deutsche Forschungsgemeinschaft under Grant No. BL-923/1. Th.V. is supported by the Helmholtz-Gemeinschaft (HGF, VH-NG 406) and the Zukunftskolleg der Universität Konstanz.

[1] W. Götze, J. Phys. Condens. Matter **11**, A1 (1999).
[2] W. Götze, *Complex Dynamics of Glass-Forming Liquids* (Oxford University Press, 2009).
[3] P. Lunkenheimer, U. Schneider, R. Brand, and A. Loidl, Contemp. Phys. **41**, 15 (2000).
[4] U. Schneider, R. Brand, P. Lunkenheimer, and A. Loidl, Phys. Rev. Lett. **84**, 5560 (2000).
[5] T. Blochowicz and E. A. Rössler, Phys. Rev. Lett. **92**, 225701 (2004).
[6] E. Ritter von Schweidler, Ann. Phys. (Leipzig) **24**, 711 (1907).
[7] B. Frick, B. Farago, and D. Richter, Phys. Rev. Lett. **64**, 2921 (1990).
[8] W. Petry, E. Bartsch, F. Fujara, M. Kiebel, H. Sillescu, and B. Farago, Z. Phys. B **83**, 175 (1991).
[9] C. Dreyfus, M. J. Lebon, H. Z. Cummins, J. Toulouse, B. Bonello, and R. M. Pick, Phys. Rev. Lett. **69**, 3666 (1992); **76**, 1763(E) (1996).
[10] Y. Yang and K. A. Nelson, Phys. Rev. Lett. **74**, 4883 (1995).
[11] Y. Yang and K. A. Nelson, J. Chem. Phys. **104**, 5429 (1996).
[12] J. Wiedersich, N. V. Surovtsev, and E. Rössler, J. Chem. Phys. **113**, 1143 (2000).
[13] S. V. Adichtchev, St. Benkhof, Th. Blochowicz, V. N. Novikov, E. Rössler, Ch. Tschirwitz, and J. Wiedersich, Phys. Rev. Lett. **88**, 055703 (2002).
[14] S. Adichtchev, T. Blochowicz, C. Tschirwitz, V. N. Novikov, and E. A. Rössler, Phys. Rev. E **68**, 011504 (2003).
[15] L. Comez, S. Corezzi, G. Monaco, R. Verbeni, and D. Fioretto, Phys. Rev. Lett. **94**, 155702 (2005).
[16] V. Bercu, M. Martinelli, C. A. Massa, L. A. Pardi, E. A. Rössler, and D. Leporini, J. Chem. Phys. **129**, 081102 (2008).
[17] W. Götze and M. R. Mayr, Phys. Rev. E **61**, 587 (2000).
[18] A. Bartsch, K. Rätzke, A. Meyer, and F. Faupel, Phys. Rev. Lett. **104**, 195901 (2010).
[19] D. Kivelson and G. Tarjus, J. Non-Cryst. Solids **235–237**, 86 (1998).
[20] W. Götze and L. Sjögren, Z. Phys. B **65**, 415 (1987).
[21] W. M. Du, G. Li, H. Z. Cummins, M. Fuchs, J. Toulouse, and L. A. Knauss, Phys. Rev. E **49**, 2192 (1994).
[22] G. Hinze, D. D. Brace, S. D. Gottke, and M. D. Fayer, J. Chem. Phys. **113**, 3723 (2000).
[23] C. Alba-Simionesco and M. Krauzman, J. Chem. Phys. **102**, 6574 (1995).

[24] C. Alba-Simionesco, V. Krakoviack, M. Krauzman, P. Migliardo, and F. Romain, J. Raman Spectrosc. **27**, 715 (1996).
[25] V. Krakoviack, C. Alba-Simionesco, and M. Krauzman, J. Chem. Phys. **107**, 3417 (1997).
[26] V. Krakoviack and C. Alba-Simionesco, J. Chem. Phys. **117**, 2161 (2002).
[27] W. Götze and Th. Voigtmann, Phys. Rev. E **61**, 4133 (2000).
[28] S. M. Bhattacharyya, B. Bagchi, and P. G. Wolynes, Phys. Rev. E **72**, 031509 (2005).
[29] S.-H. Chong, Phys. Rev. E **78**, 041501 (2008).
[30] S.-H. Chong, S.-H. Chen, and F. Mallamace, J. Phys. Condens. Matter **21**, 504101 (2009).
[31] S. H. Chen, Y. Zhang, M. Lagi, S. H. Chong, P. Baglioni, and F. Mallamace, J. Phys. Condens. Matter **21**, 504102 (2009).
[32] M. E. Cates and S. Ramaswamy, Phys. Rev. Lett. **96**, 135701 (2006).
[33] M. Greenall and M. E. Cates, Phys. Rev. E **75**, 051503 (2007).
[34] P. Mayer, K. Miyazaki, and D. R. Reichman, Phys. Rev. Lett. **97**, 095702 (2006).
[35] C. A. Angell, L. Boehm, M. Oguni, and D. L. Smith, J. Mol. Liq. **56**, 275 (1993).
[36] M. Zhao, L. Jin, B. Chen, Y. Ding, H. Ma, and D. Chen, Appl. Opt. **42**, 4031 (2003).
[37] A. Brodin and E. A. Rössler, J. Phys. Condens. Matter **18**, 8481 (2006).
[38] L. N. G. Filon, Proc. R. Soc. Edinburgh **49**, 38 (1929).
[39] E. O. Tuck, Math. Comput. **21**, 239 (1967).
[40] J.-P. Hansen and I. R. McDonald, *Theory of Simple Liquids*, 3rd ed. (Academic Press, 2006).
[41] H. Z. Cummins, J. Phys. Condens. Matter **17**, 1457 (2005).
[42] W. Götze, A. P. Singh, and Th. Voigtmann, Phys. Rev. E **61**, 6934 (2000).
[43] J. Wuttke, M. Ohl, M. Goldammer, S. Roth, U. Schneider, P. Lunkenheimer, R. Kahn, B. Rufflé, R. Lechner, and M. A. Berg, Phys. Rev. E **61**, 2730 (2000).
[44] A. Brodin, R. Bergman, J. Mattsson, and E. A. Rössler, Eur. Phys. J. B **36**, 349 (2003).
[45] U. Bengtzelius, W. Götze, and A. Sjölander, J. Phys. C **17**, 5915 (1984).
[46] E. Leutheusser, Phys. Rev. A **29**, 2765 (1984).
[47] R. M. Pick, T. Franosch, A. Latz, and C. Dreyfus, Eur. Phys. J. B **31**, 217 (2003); **31**, 229 (2003).
[48] *Broadband Dielectric Spectroscopy*, edited by F. Kremer and A. Schönhals (Springer, 2003).
[49] M. Fuchs, I. Hofacker, and A. Latz, Phys. Rev. A **45**, 898 (1992).
[50] Th. Voigtmann, A. M. Puertas, and M. Fuchs, Phys. Rev. E **70**, 061506 (2004).
[51] Th. Voigtmann, Phys. Rev. E **68**, 051401 (2003).
[52] F. Weysser, A. M. Puertas, M. Fuchs, and Th. Voigtmann, Phys. Rev. E **82**, 011504 (2010).
[53] T. Franosch, M. Fuchs, W. Götze, M. R. Mayr, and A. P. Singh, Phys. Rev. E **56**, 5659 (1997).
[54] R. Schilling and T. Scheidsteger, Phys. Rev. E **56**, 2932 (1997).
[55] S.-H. Chong, W. Götze, and A.-P. Singh, Phys. Rev. E **63**, 011206 (2000).
[56] S.-H. Chong and W. Götze, Phys. Rev. E **65**, 041503 (2002); **65**, 051201 (2002).
[57] R. Zwanzig, Phys. Rev. **124**, 983 (1961); H. Mori, Prog. Theor. Phys. **34**, 399 (1965).
[58] G. Szamel and E. Flenner, Europhys. Lett. **67**, 779 (2004).
[59] W. Götze, in *Liquids, Freezing and Glass Transition (Les Houches, Session LI)*, edited by J. P. Hansen, D. Levesque, and J. Zinn-Justin (North-Holland, Amsterdam, 1991).
[60] G. Williams and J. Fournier, J. Chem. Phys. **104**, 5690 (1996).
[61] J. F. Douglas and J. B. Hubbard, Macromolecules **24**, 3163 (1991).
[62] L. Sjörgen, Physica A **322**, 81 (2003).
[63] W. Feller, *An Introduction to Probability Theory and Its Applications*, 3rd ed., Vol. I (Wiley & Sons, New York, 1968).
[64] M. Tokuyama and H. Mori, Prog. Theor. Phys. **55**, 411 (1976).
[65] M. Tokuyama, Physica A **387**, 1926 (2008).
[66] W. Götze and T. Voigtmann, Phys. Rev. E **67**, 021502 (2003).
[67] K. S. Schweizer and E. J. Saltzman, J. Chem. Phys. **119**, 1181 (2003); K. S. Schweizer, *ibid*. **123**, 244501 (2005).
[68] G. Brambilla, D. El Masri, M. Pierno, L. Berthier, L. Cipelletti, G. Petekidis, and A. B. Schofield, Phys. Rev. Lett. **102**, 085703 (2009); J. Reinhardt, F. Weysser, and M. Fuchs, *ibid*. **105**, 199604 (2010); G. Brambilla, D. El Masri, M. Pierno, L. Berthier, and L. Cipelletti, *ibid*. **105**, 199605 (2010).
[69] L. Sjögren, Phys. Rev. A **33**, 1254 (1986).
[70] A. Heesemann, V. Zöllmer, K. Rätzke, and F. Faupel, Phys. Rev. Lett. **84**, 1467 (2000).
[71] J. Gapiski, W. Steffen, A. Patkowski, A. P. Sokolov, A. Kisliuk, U. Buchenau, M. Russina, F. Mezei, and H. Schober, J. Chem. Phys. **110**, 2312 (1999).
[72] R. Kohlrausch, Pogg. Ann. **167**, 56 (1854).
[73] M. Fuchs, J. Non-Cryst. Solids **172–174**, 241 (1994).
[74] U. Schneider, P. Lunkenheimer, R. Brand, and A. Loidl, Phys. Rev. E **59**, 6924 (1999).
[75] L. Börjesson, M. Elmroth, and L. M. Torell, Chem. Phys. **149**, 209 (1990).
[76] M. Domschke, Diploma thesis, Technische Universität Darmstadt, 2008.
[77] T. Blochowicz, A. Brodin, and E. A. Rössler, Adv. Chem. Phys. **133**, 127 (2006).
[78] A. Kudlik, S. Benkhof, T. Blochowicz, C. Tschirwitz, and E. Rössler, J. Mol. Struct. **479**, 201 (1999).
[79] K. L. Ngai and M. Paluch, J. Chem. Phys. **120**, 857 (2004).
[80] G. P. Johari and M. Goldstein, J. Chem. Phys. **53**, 2372 (1970).